Protein fibrillogenesis model tracked by its intrinsic TRES

Li Hung C. Chung,[1] David J. S. Birch,[1] Vladislav Vyshemirsky,[2] Angelo Bella,[3] Maxim G. Ryadnov,[3] and Olaf J. Rolinski[1*]

[1]Photophysics Group, Centre for Molecular Nanometrology, Department of Physics, Scottish Universities Physics Alliance, University of Strathclyde, 107 Rottenrow, Glasgow G4 0NG, UK

[2]School of Mathematics and Statistics, University of Glasgow, Glasgow G12 8QQ, UK

[3]National Physical Laboratory, Hampton Road, Teddington, TW11 0LW, UK

The excited-state kinetics of the fluorescence of tyrosine in a de novo protein fibrillogenesis model was investigated as a potential tool for monitoring protein fibre formation and complexation with glucose (glycation). In stark contrast to insulin the time-resolved emission spectra (TRES) recorded over the period of 700 hours in buffered solutions of the model with and without glucose revealed no apparent changes in Tyr fluorescence responses. This indicates the stability of the model and provides a measurement-supported basis for its use as a reference material in fluorescence studies of protein aggregation.

* Electronic mail: o.j.rolinski@strath.ac.uk

I. INTRODUCTION

There is a significant interest in improving the understanding of protein fibrillogenesis. The process is fundamentally important for normal and pathological phenomena including those that underpin the onset of neurodegenerative diseases such as Alzheimer's disease (AD), Parkinson's disease (PD) and diabetes mellitus type II.[1,2] These are proteopathic disorders, in which precursor protein undergoes abnormal development via a chain of conformational changes resulting in the formation of amyloid fibrils. Amyloid aggregation is structurally polymorphic due to the different assembly pathways monomeric units are involved in.[3] As a result, the units can assemble into different populations of oligomeric forms characterised by varied growth kinetics. In contrast, normal fibrillogenesis processes, such as those supporting the assembly of actin filaments or collagen and fibrin fibrils, exhibit more homogenous growth rates. To better understand the rate of fibrillogenesis, it is advantageous if the complexity of natural proteins is reduced and fibrillogenesis studies performed using simplistic and reproducible models first. Such models can be based on well-established rules of sequence-to-structure relationships and offer necessary predictability in control over fibrillogenesis at the molecular level. To achieve this, the approach requires a well-characterised protein folding element.

One of such elements is an α-helical coiled coil, which is characteristic of about 5-10% of all amino acids in proteins. The sequence-to-structure relationships for this motif are reasonably well understood and have been validated in many designs.[4] The hallmark of canonical alpha-helical coiled coils is a heptad repeat of hydrophobic (***H***) and polar (***P***) residues, ***HPPHPPP***, which is usually designated as ***abcdefg***. This arrangement gives rise to a rope-like bundle of two or more helices interdigitated with the formation of a contiguous hydrophobic interface, with each helix having 3.5 amino-acid residues per turn. Charged residues in ***g*** and ***e*** sites stabilise the bundle further via bridging electrostatic interactions.[5]

Using these principles a coiled-coil sequence was designed to assemble into filamentous structures from the monomer up.[6] The sequence – KLAALKQKLAALKKELAALEQELAALEQ – was shown to adopt a sticky-ended coiled coil oligomer that propagates longitudinally into relatively uniform filaments of 2.7 ± 0.3 μm in length. In contrast to amyloid-like fibrils, this assembly is characterised by homogenous growth kinetics, with individual fibres exhibiting the same growth rates at both growing ends, i.e. N and C-termini. By labelling the peptide with an Alexa Fluor 488 dye it was possible to monitor the process of fibrillogenesis in real time by structured illumination microscopy (SIM) in solution under static, equilibrium conditions,[6] and under non-equilibrium conditions by applying the coffee ring effect[7]. Under both conditions, the assembly starts with a seeding or initiation phase of folded monomeric units, followed by a stabilization phase of laterally equilibrated assemblies, and a maturation phase of longitudinally equilibrated assemblies at which fibre formation is essentially complete.

However, extrinsic fluorophores such as Alexa Fluor 488 require covalent conjugation with the peptide sequence and once incorporated could in principle interfere with fibrillogenesis[8]. Here we probed the feasibility of using an intrinsic fluorophore and replace the lysyl residue in position 14, which was used as a fluorophore labelling site, with a tyrosyl residue (see Fig. 1). A single tyrosine (Tyr) in each monomer and the lack of tryptophan allows for selective excitation without the complication of energy transfer. Tyr is known to be sensitive to local microenvironments e.g. in evolving insulin,[9] during the process of glycation as shown in this paper and in the aggregation of beta-amyloid[10]. Therefore, we reason that the fluorescence response of the residue, both steady-state

and time-resolved, can be used to monitor fibrillogenesis. In addition, complementary information can be obtained using the same approach with regards to complexation with sugar molecules (glycation).

Protein glycation is a non-enzymatic process, which occurs as a post-folding modification affecting protein stability, structure and function. In amyloid deposits, protein is often glycated which suggests a correlation between fibrillogenesis and glycation[11].

Both the self-assembly of the peptide into fibres and their potential complexation with glucose were studied using time-resolved emission spectra (TRES). TRES is a series of the fluorescence emission spectra emitted at discrete times after pulse excitation on the nanosecond time scale. Changes in TRES of the sample determined and measured over several days were used to correlate with the processes of fibrillogenesis and glycation.

II. EXPERIMENTAL

The peptide was assembled on a Fmoc-Gln(Trt)-Wang resin using a PTI Tribute peptide synthesizer. HBTU/DIPEA and piperidine were used as coupling and deprotection reagents, respectively. After the synthesis, the peptide was cleaved from the resin following a 2-hour treatment with the cleavage cocktail of 95% TFA, 2.5% TIS, 2.5%. Diethyl ether was added to the mixture to precipitate and wash the peptide, which was followed by centrifugation at 6,500 rpm (20 min, 3 times). The pellet was then purified by a Dionex UltiMate 3000 HPLC system using a semi-preparative column (ACE 5C18-300 250x10 mm) at a flow rate of 3.5 mL/min. The purity of the peptide was confirmed by analytical HPLC (ACE 5C18-300 250x4.6 mm column; at a flow rate of 1 mL/min) and the identity was confirmed by MALDI-ToF mass spectrometry: MS $[M + H]^+$: m/z 3068.6 (calculated), 3068.6 (observed).
Aqueous peptide solutions (300 µL, 50 µM) were prepared in filtered (0.22 µm) 10 mM MOPS, pH 7.4, and incubated overnight at room temperature for fibrillogenesis. The fluorescence of the peptide was measured at 37.5°C, pH 7.4 to mimic physiological conditions. For comparative measurements bovine insulin (Sigma-Aldrich) was used without further purification. 50 uM solution of bovine insulin in PBS (0.01 M). A stock solution of D-(+)-Glucose (Sigma-Aldrich) in distilled water was added to the peptide and insulin where the final concentration of glucose was 50 mM.

Absorption and fluorescence intensity measurements were performed using Lambda 25 (Perkin Elmer) and Fluorolog (Horiba Scientific), respectively. Time-resolved fluorescence decays were taken on the DeltaFlex fluorescence lifetime system (Horiba Jobin Yvon IBH Ltd, Glasgow) using time correlated single photon counting. A NanoLED with a wavelength of 279 nm and producing pulses of ~600 ps was used for excitation[12]. Fluorescence decays were measured with varying detection wavelengths from 290 to 340 nm in 5 nm increments. The decays were fitted to a three-exponential model function for each detection wavelength:

$$I_\lambda(t) = \sum_{i=1}^{3} \alpha_i(\lambda) \exp\left(\frac{-t}{\tau_i(\lambda)}\right) \qquad (1)$$

The parameters $\tau_i(\lambda)$ is the fluorescence lifetime and $\alpha_i(\lambda)$ is the i^{th} pre-exponential component. The parameters were recovered to generate TRES according to[9]:

$$I_t(\lambda) = \frac{I_\lambda(t)\, S(\lambda)}{\sum_i \alpha_i(\lambda)\tau_i(\lambda)} \qquad (2)$$

$S(\lambda)$ is the emission intensity from the sample and the denominator represents the total emitted photons from the fluorescence sample. TRES were then converted to functions of the wavenumbers $I_t(v)$ according to:

$$I_t(v) = \lambda^2 I_t(\lambda) \qquad (3)$$

Using the Toptygin-type representation of the TRES[13] we model $I_t(v)$ by the function:

$$F(v) = \sum_{i=1}^{N} \frac{C_i}{\sqrt{2\pi}\, v_i \sigma_i \left(v_i^2 + 3\sigma_i^2\right)} v^3 \, exp\left(\frac{-(v - v_i)^2}{2\sigma_i^2}\right) \qquad (4)$$

where the expression $\left(\sqrt{2\pi}\, v_i \sigma_i \left(v_i^2 + 3\sigma_i^2\right)\right)^{-1}$ for each component *i* is the normalisation factor of the $v^3 \exp\left[\frac{-(v-v_i)^2}{2\sigma_i^2}\right]$ function. Thus, C_i coefficient represents fluorescence contribution of the i^{th} component.

III. RESULTS AND DISCUSSION

Steady state absorption spectra measured for peptide samples at different times after preparation over nearly 700 hours are shown in Fig. 2A. The spectra are dominated by the tyrosine peak absorbance around 279 nm and show increasing effect of Rayleigh scattering with sample ageing up to about 450 hours and then gradual drop in absorbance. At the same period of time, the intensities of fluorescence spectra (Fig. 2B) have increased (integrated intensities shown in Fig. 2C) again up to 450 hours, with the shape of the spectra changing insignificantly (Fig. 2D), and then started to decrease. The growing contributions of the scattered light in the absorption spectra are indicative of oligomeric forms increasing in size,[14] while increases in fluorescence intensity may be attributed to a higher quantum yield of tyrosine caused by its gradually decreasing quenching by water.[15] Both observations are consistent with the fibrillogenesis process over the studied period. The potential cause of the decreased intensities observed in both spectra is likely to be caused by precipitation of the larger fibrils and, consequently, decreasing concentration of the fluorescent material in the solution.

In the next stage fibrillogenesis was monitored by means of the potential changes in the fluorescence intensity decay of Tyr residues. The full set of fluorescence intensity decays for the fibrillating sample was measured at wavelengths from 290 nm to 340 nm with 5 nm increments. The series of measurements started at a seeding phase in the first 20 min (0.33 h) of sample preparation, with subsequent measurements recorded at 22, 43, 68, 95, 201, 312, 381, 454, 527, 600 and 693 hours.

Fig. 3 presents fluorescence intensity decays recorded at different time points and wavelengths. Fluorescence intensity decays recorded at the longer wavelengths show the progressive emergence of

a longer decay component, as illustrated in Fig. 3A and B for the earliest (0.33 h) and latest (693 h) samples, respectively. This observation is consistent with protein wavelength-lifetime dependence[9,16] which may be explained by the dielectric relaxation of the fluorophores or by the presence of multiple components of different emission spectra and fluorescence lifetimes increasing with emission wavelengths. However a substantial contribution of the scattered excitation light in the decay signal can also preferentially distort the decay at shorter wavelengths. In order to separate the scattered light from the actual fluorescence decays, we used for the data fitting the model decays consisting of the both multi-exponential part and the scattered light component.[17] Tables 1-5 in Supplementary Material (SM) show parameters recovered from fitting the 3-exponential model to the data measured for the 0.33, 43, 312, 454 and 693 hours old samples respectively, together with the percentage contributions of the scattered light $Sc(\lambda)$ at each detection wavelength λ. Increased contributions of the scattered light were detected in the decays measured at 290 nm due to close distance between the excitation and detection wavelength and picking up the excitation light by the detector even at low scatter from the sample. We note that due to structural complexity of the sample during fibrillogenesis (distribution in fibril's sizes and structure) and potential effects of dielectric relaxation, the individual fluorescence decays cannot be resolved by means of any specific model of kinetics. Instead, the 3-exponential representations of these decays were used to produce TRES.

For the protein model, the TRES representation $v^{-3}I_t(v)$ and normalised $v^{-3}I_t(v)$ were plotted for different times after preparation. A few samples of age 0.33, 43 and 693 hours are shown in Fig. 4A, C, and E. The fluorescence spectra measured at all stages of fibrillization decay gradually and, at the same time, shifts towards smaller wavenumbers (which is better seen in the normalised spectra, Fig. 4B, D and F). The detailed analysis of the spectra indicates presence of two fluorescent forms with emission peaks at ~33,000 and ~31,500 cm^{-1} and the effects of dielectric relaxation in both forms. However, the effect of dielectric relaxation is relatively small (~500 cm^{-1}). Indeed, the comparison of the observed TRES response of Tyr in the protein model with the significant Tyr TRES changes observed in insulin (Fig. 4G, H) indicate high stability of the Tyr surroundings in the model peptide.

To further examine the stability features of the fibrillogenesis model, glucose was added to the sample to investigate potential glycation effects. The peptide model was also incubated with glucose for nearly 700 hours and the examples of TRES for 0.58, 48, and 693 hours are shown in 5A, C and E, respectively. For the sample 0.58 hours old, at 34,500 cm^{-1} the points are outliers after each moment of excitation which may be heavily influenced from light scattering as it is close to the excitation wavelength (279 nm). The normalised TRES (Fig 5B, D and F) show again small changes within the TRES when glucose is present at 48 hours and 693 hours of incubation. As expected (the peptide has no binding sites for glucose) no evidence of TRES changes was observed over time, demonstrating that the protein model is not prone to glycation.

For comparison, Fig. 4G, H and 5G, H show the effect glucose has on insulin after 693 hours. In fact, insulin's TRES evolves over time due to insulin aggregation (data not shown), but glycation substantially modifies this evolution. Free insulin undergoes drastic spectral changes due to excitation triggered conformational changes of insulin. When insulin has been incubated with glucose for 693 hours, there is a no spectral change after excitation which indicates that there is no conformational change and that the structure is rigid. The main targets of glycation are arginine, lysine, cysteine residues, and N-terminus of amino groups. For bovine insulin, glycation occurs on Lys (B29) and on N-terminus of chains A and B[18].

To gather more information on the spectral changes for the peptide, all TRES were fitted by the distribution function (eqtn 4). It was necessary to assume N=2 to obtain a good fit, which implies the

existence of two fluorescent forms with emission maxima at ~33,000 and ~31,500 cm^{-1} (for the freshly prepared sample) evolving differently over the studied period. Fig 6A shows the shifts of spectral peak positions following the moment of excitation for the samples measured at different times after preparation, while the fluorescence contributions $C_i(t)$ of each component are shown on Fig. 6B. The curved shapes of all plots *LogI(t)* vs. time shows that the kinetics is more complex than exponential and both forms decay at similar rates.

Combined analysis of the TRES and the steady-state data seem to suggest three stages of the model fibrillogenesis: During the first 22 hours the 33,000 cm^{-1} form shifts towards shorter wavenumbers by ~500 cm^{-1} (Fig.6A) while the 31,500 cm^{-1} form shows much larger shift by ~1,500 cm^{-1}. Both shifts may be related to dielectric relaxation. Moreover, the percentage fluorescence contribution of the 33,000 cm^{-1} form increases from 63 to 90% (estimated from the initial values of $C_i(t)$ - Fig.6B), while the over decreases from 37 to 10%. During this time the initial oligomers are formed and Tyr residues experience significant changes in their local environments.

The second stage covers the period from about 24 hours to ~450 hours. At this time the positions of the spectral peaks $\nu_i(t)$and the fluorescence intensity decays $C_i(t)$ do not change significantly. The increasing intensity of the steady-state fluorescence observed during this period (Fig.2B) and no changes recorded in lifetimes can be explained by initial oligomers showing low quantum yield of fluorescence (due to static quenching by water), but become more fluorescent once incorporated into fibres.

The third stage begins after ~450 hours, when the TRES parameters remain stable and the rates of the decays $C_i(t)$ do not change substantially, but the peak intensities of the absorption and fluorescence spectra start to drop (Fig.2A nd 2B). This effect is consistent with the formation of larger forms that precipitate, which effectively reduces the concentration of fluorescent material in the sample. The process does not affect the detected fluorescence decays, which are independent of fluorophore concentration and because precipitation applies to the larger fibrils the local environments of tyrosines under measurement are unaffected. This suggestion is consistent with the increasing number of monomers in the growing fibrils. In the previous studies of the model prepared under similar conditions[6], the calculated number of monomers in a fibril was 225×10^3. Clearly the fibrillogenesis of the structures of this size is not reflected in changes of intrinsic fluorescence.

IV. CONCLUSION

In conclusion, the increased scatter and changes in fluorescence intensity observed during the whole monitored period of ~700 hours suggest an equilibrated fibrillogenesis of the model peptide, while the photophysics of the Tyr residue is not affected directly during the most of the process except for the initial stage, i.e. formation of initial oligomers during about 24 hours. Tyrosines in other peptides and proteins (e.g. insulin) report their structural changes over much longer time, which allows using the model peptide we studied as a useful reference in similar TRES experiments. Simultaneously, the fibrillogenesis model can also be probed by means of the time-resolved anisotropy of tyrosine, $r(t) = (r_0 - r_\infty)\exp\left(-\frac{t}{\tau_r}\right) + r_\infty$, where the rotational time τ_r and the final anisotropy r_∞ are likely to increase due to increasing size of the fibrils.

ACKNOWLEDGEMENTS

The authors would like to thank Jack Robertson and staff in The Burley Group for access to the equipment in order to synthesize the peptide model. LHCC would like to acknowledge the support of an NPL-Strathclyde Graduate Institute studentship.

References

[1] T.P.J. Knowles, M. Vendruscolo, and C.M. Dobson, Nat. Rev. Mol. Cell Biol. **15**, 384 (2014).

[2] D. Eisenberg and M. Jucker, Cell **148**, 1188 (2012).

[3] D.N. Woolfson and M.G. Ryadnov, Curr. Opin. Chem. Biol. **10**, 559 (2006).

[4] D.N. Woolfson, Adv. Protein Chem. **70**, 79 (2005).

[5] F.H.C. Crick, Acta Crystallogr **6**, 689 (1953).

[6] A. Bella, M. Shaw, S. Ray, and M.G. Ryadnov, Sci. Rep. **4**, 7529 (2014).

[7] M. Shaw, A. Bella, and M.G. Ryadnov, J. Phys. Chem. Lett. **8**, 4846 (2017).

[8] Y. Porat, A. Abramowitz, and E. Gazit, Chem. Biol. Drug Des. **67**, 27 (2006).

[9] L.H.C. Chung, D.J.S. Birch, V. Vyshemirsky, M.G. Ryadnov, and O.J. Rolinski, Appl. Phys. Lett. **111**, 263701 (2017).

[10] A. Alghamdi, V. Vyshemirsky, D.J.S. Birch, and O.J. Rolinski, Methods Appl. Fluoresc. **6**, 024002 (2018).

[11] G. Münch, H.J. Lüth, A. Wong, T. Arendt, E. Hirsch, R. Ravid, and P. Riederer, J. Chem. Neuroanat. **20**, 253 (2000).

[12] C.D. McGuiness, K. Sagoo, D. McLoskey, and D.J.S. Birch, Meas. Sci. Technol. **15**, 19 (2004).

[13] D. Toptygin and L. Brand, Chem. Phys. Lett. **322**, 496 (2000).

[14] J. Pellaud, U. Schote, T. Arvinte, and J. Seelig, J. Biol. Chem. **274**, 7699 (1999).

[15] R. McGuire and I. Feldman, Photochem. Photobiol. **18**, 119 (1973).

[16] O.J. Rolinski, D. McLaughlin, D.J.S. Birch, and V. Vyshemirsky, Methods Appl. Fluoresc. **4**, 024001 (2016).

[17] O.J. Rolinski, T. Wellbrock, D.J.S. Birch, and V. Vyshemirsky, J. Phys. Chem. Lett. **6**, 3116 (2015).

[18] C. Iannuzzi, G. Irace, and I. Sirangelo, Front. Mol. Biosci. **1**, 1 (2014).

Figures captions:

Figure 1: Fibrillogenesis model design. (A) The linear amino-acid sequence of the protein model, three copies of which form a staggered coiled-coil unit with cationic and anionic overhangs, each having two heptads. (B) The unit configured into coiled-coil helical wheels with 3.5 residues per turn. (C) A ribbon diagram of the staggered unit (PDB 3L4F entry rendered with PyMol). (D) A schematic representation of the longitudinal propagation of the unit into a contiguous coiled coil. For clarity only one coiled coil is shown: resulting fibrils are bundles of individual coiled coils. Key: cationic and anionic heptads and residues are shown in blue and red, respectively. Double-headed arrows indicate electrostatic interactions between lysines and glutamates. One of the two combinations of interactions, highlighted by bold and dashed arrows, can be formed within one coiled coil unit. Asterisks indicate the Tyr residue.

Figure 2: Steady state measurements A) absorbance and B) emission of the protein fibrillogenesis model for 0, 22, 43, 68, 95, 201, 312, 381, 454, 527, 600 and 693 hours after sample preparation. The integrated fluorescence intensity C) and normalised emission spectra D) were also plotted.

Figure 3: The instrumental pulse profile (black) and fluorescence intensity decays for detection wavelengths of 290, 295, 300, 305, 310, 315, 320, 325, 330, 335 and 340 nm for A) 0.33 and B) 693 hours after sample preparation of fibrillogenesis model.

Figure 4: The left hand panel show the TRES spectra of the peptide model (A, C, E) and insulin (G) for 0.33, 43, and 693 hours respectively. The right hand panel shows the normalised TRES plots for the free peptide model (B, D, F) and insulin (H). The plots were determined at 0, 0.25, 0.5, 0.75, 1, 1.5, 2, 3, 4, 5, 6, 7, 8, 9, and 10 ns after excitation. 0 ns is taken out of 0.33 hours of the peptide model and 693 hours of insulin due to high scatter.

Figure 5: The left hand panel show the TRES spectra of the peptide model (A, C, E) and insulin (G) in the presence of glucose at times 0.58, 48, and 693 hours respectively. The right hand panel shows the normalised TRES plots for the free peptide model (B, D, F) and insulin (H). The plots were determined at 0, 0.25, 0.5, 0.75, 1, 1.5, 2, 3, 4, 5, 6, 7, 8, 9, and 10 ns after excitation. 0 ns is taken out of 0.58 hours data due to high scatter.

Figure 6: TRES parameters taken from the 2 Gaussian models of peak positions vi and the corrected fluorescence contributions Ci fitted to two exponential models. Fluorescent species 1 (■) and 2 (●) where measured at 0.33, 22, 43, 68, 95, 201, 312, 381, 454, 527, 600, 693 hours after sample preparation.

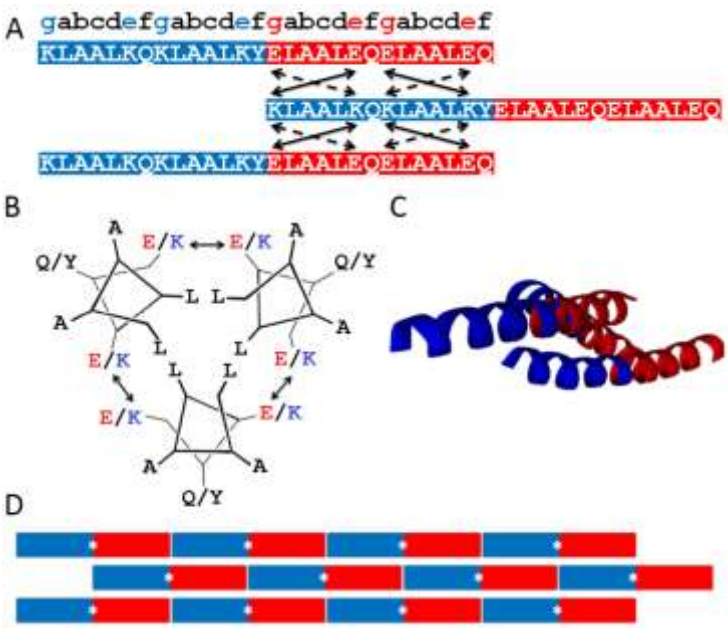

Figure 1: Fibrillogenesis model design. (A) The linear amino-acid sequence of the protein model, three copies of which form a staggered coiled-coil unit with cationic and anionic overhangs, each having two heptads. (B) The unit configured into coiled-coil helical wheels with 3.5 residues per turn. (C) A ribbon diagram of the staggered unit (PDB 3L4F entry rendered with PyMol). (D) A schematic representation of the longitudinal propagation of the unit into a contiguous coiled coil. For clarity only one coiled coil is shown: resulting fibrils are bundles of individual coiled coils. Key: cationic and anionic heptads and residues are shown in blue and red, respectively. Double-headed arrows indicate electrostatic interactions between lysines and glutamates. One of the two combinations of interactions, highlighted by bold and dashed arrows, can be formed within one coiled coil unit. Asterisks indicate the Tyr residue.

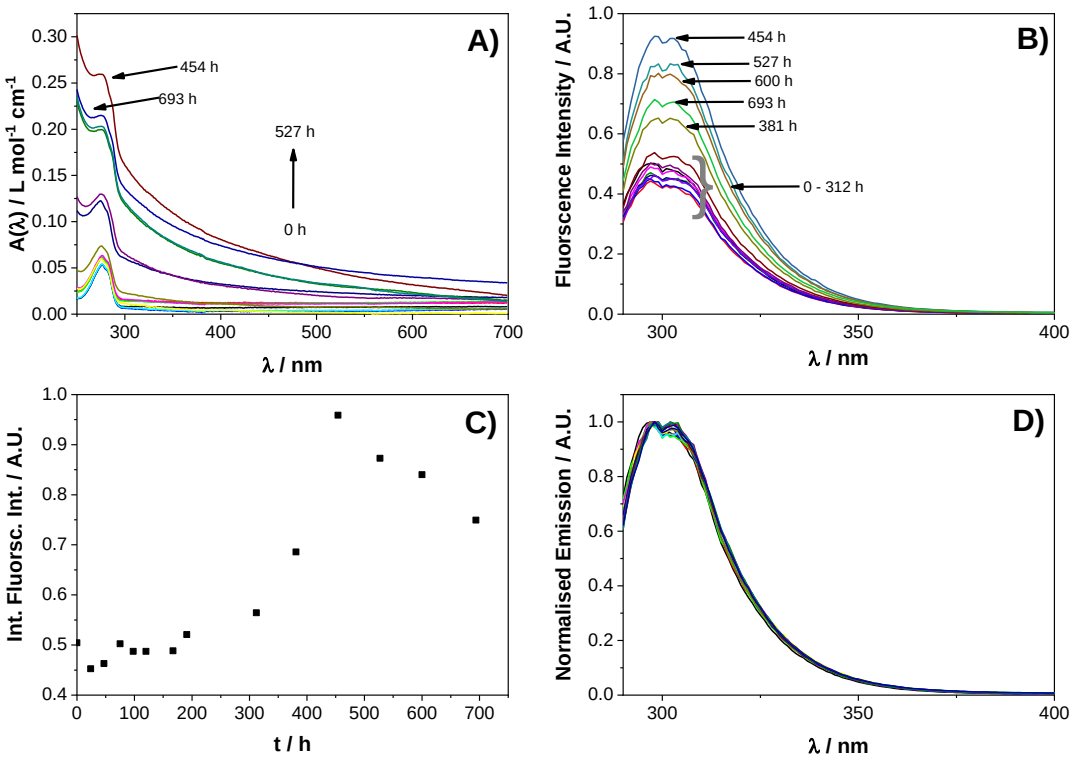

Figure 2: Steady state measurements A) absorbance and B) emission of the protein fibrillogenesis model for 0, 22, 43, 68, 95, 201, 312, 381, 454, 527, 600 and 693 hours after sample preparation. The integrated fluorescence intensity C) and normalised emission spectra D) were also plotted.

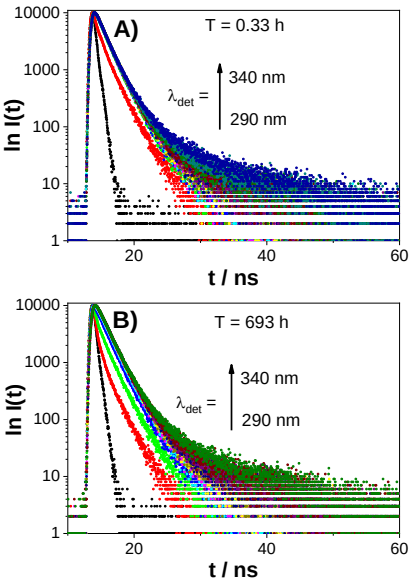

Figure 3: The instrumental pulse profile (black) and fluorescence intensity decays for detection wavelengths of 290, 295, 300, 305, 310, 315, 320, 325, 330, 335 and 340 nm for A) 0.33 and B) 693 hours after sample preparation of fibrillogenesis model.

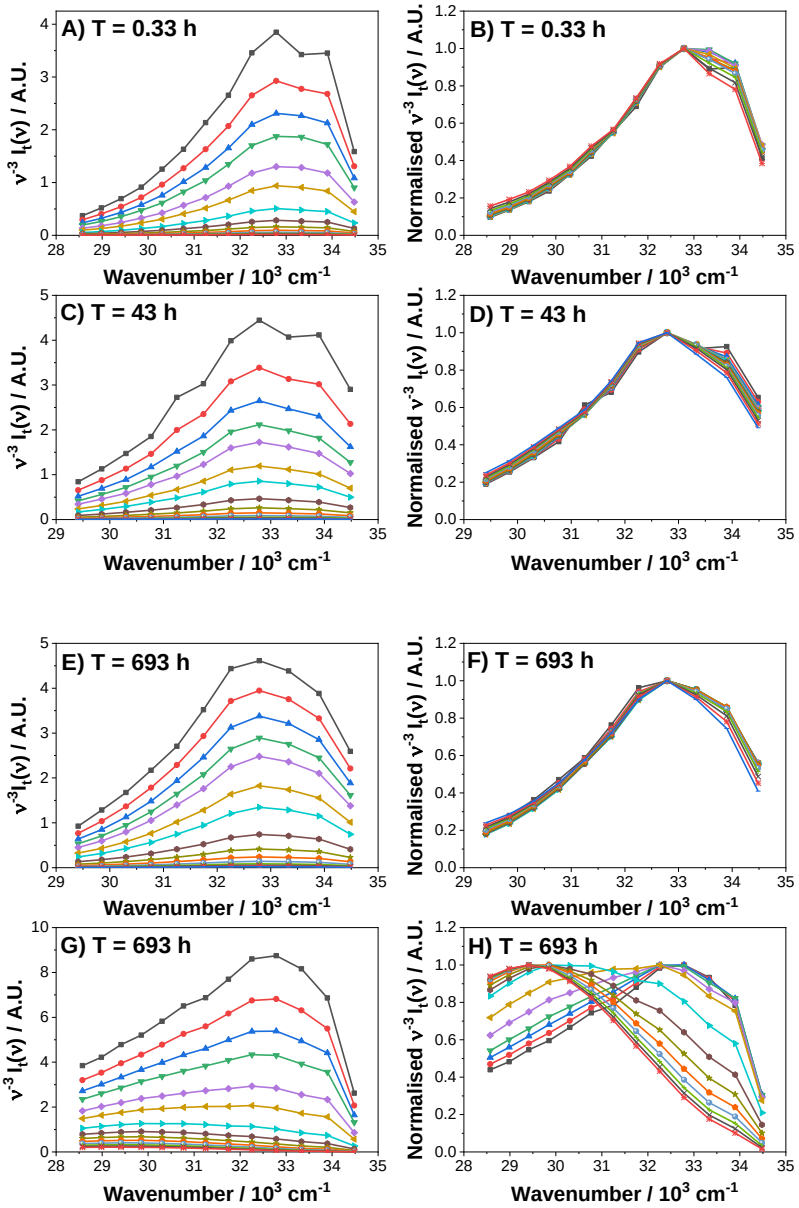

Figure 4: The left hand panel show the TRES spectra of the peptide model (A, C, E) and insulin (G) for 0.33, 43, and 693 hours respectively. The right hand panel shows the normalised TRES plots for the free peptide model (B, D, F) and insulin (H). The plots were determined at 0, 0.25, 0.5, 0.75, 1, 1.5, 2, 3, 4, 5, 6, 7, 8, 9, and 10 ns after excitation. 0 ns is taken out of 0.33 hours of the peptide model and 693 hours of insulin due to high scatter.

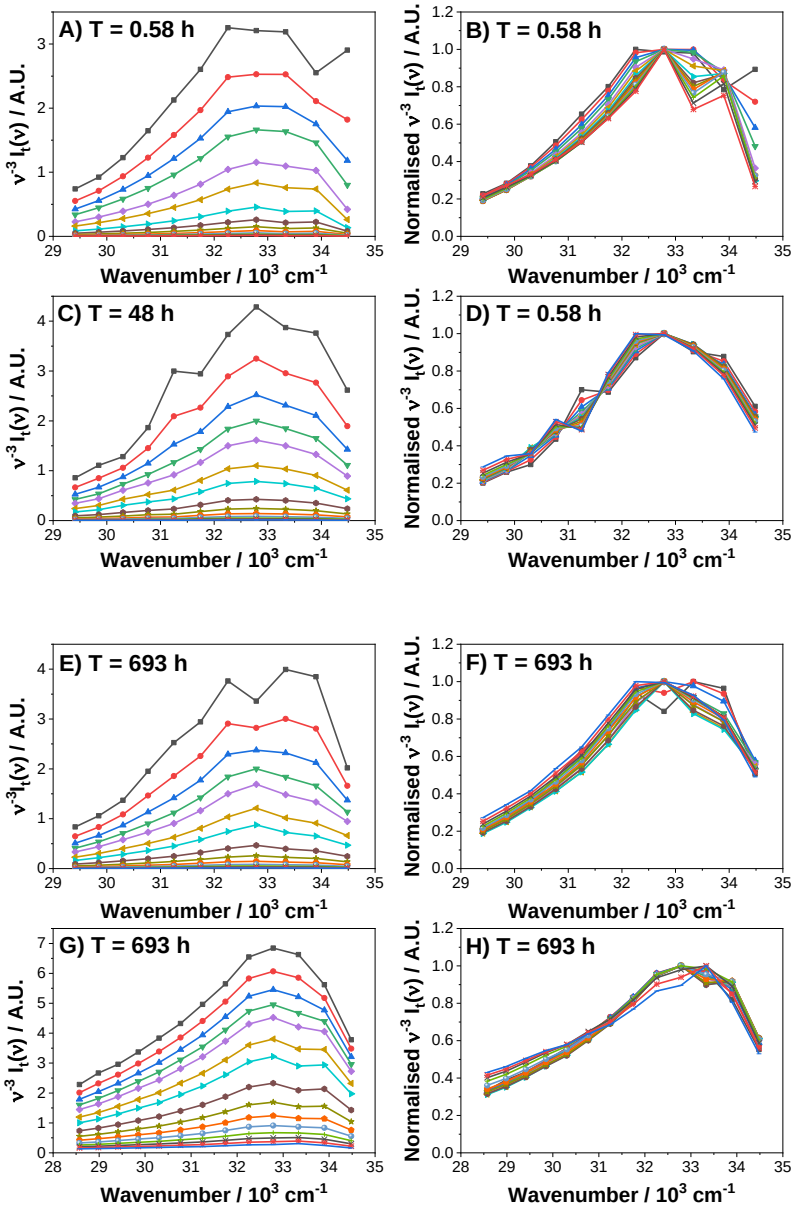

Figure 5: The left hand panel show the TRES spectra of the peptide model (A, C, E) and insulin (G) in the presence of glucose at times 0.58, 48, and 693 hours respectively. The right hand panel shows the normalised TRES plots for the free peptide model (B, D, F) and insulin (H). The plots were determined at 0, 0.25, 0.5, 0.75, 1, 1.5, 2, 3, 4, 5, 6, 7, 8, 9, and 10 ns after excitation. 0 ns is taken out of 0.58 hours data due to high scatter.

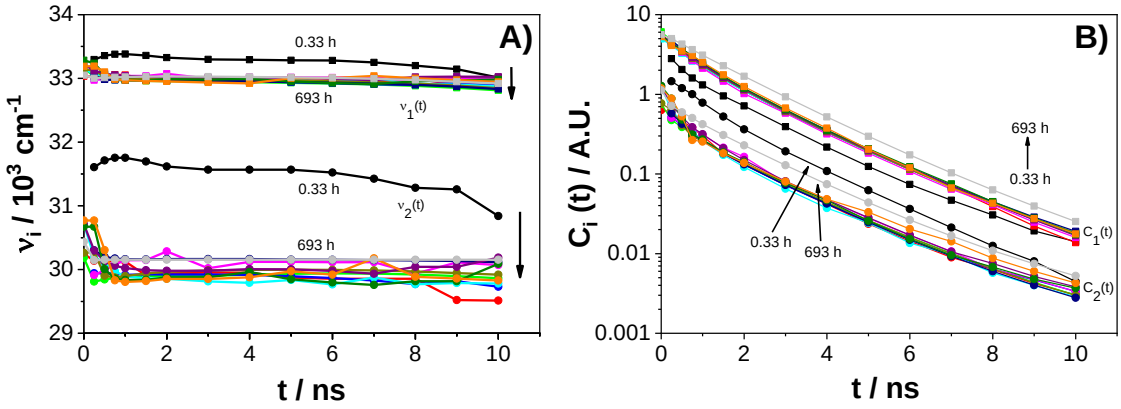

Figure 6: TRES parameters taken from the 2 Gaussian models of peak positions ν_i and the corrected fluorescence contributions C_i fitted to two exponential models. Fluorescent species 1 (■) and 2 (●) where measured at 0.33, 22, 43, 68, 95, 201, 312, 381, 454, 527, 600, 693 hours after sample preparation.

Protein fibrillogenesis model tracked by its intrinsic TRES

Li Hung C. Chung, David J. S. Birch, Vladislav Vyshemirsky, Angelo Bella, Maxim G. Ryadnov and Olaf J. Rolinski*

SUPPLEMENTARY MATERIAL

Table 1: Lifetime data extracted from 0.33 hours of ageing fibrillogenesis model including lifetime values (T1, T2, T3), pre-exponential values (A1, A2, A3), scatter component (Sc), χ^2, and absorbance values for each corresponding wavelength.

Wavelength / nm	T1 / ns	A1 / %	T2 / ns	A2 / %	T3 / ns	A3 / %	Sc / %	χ^2
290	0.02	95.68	1.04	2.78	2.11	1.54	36.82	1.29
295	0.49	39.29	1.51	53.94	2.84	6.77	0.00	1.3
300	0.81	49.78	1.84	49.74	6.68	0.48	4.58	1.14
305	0.39	39.77	1.54	56.74	3.59	3.49	13.39	1.07
310	0.43	40.11	1.57	57.01	3.85	2.88	2.77	1.05
315	0.50	39.43	1.62	58.25	4.20	2.32	4.73	1.19
320	0.45	43.52	1.63	54.77	4.58	1.71	1.15	1.17
325	0.50	40.44	1.64	57.61	4.63	1.95	5.04	1.11
330	0.44	40.98	1.58	56.44	4.24	2.58	6.37	1.39
335	0.56	40.40	1.69	58.06	5.43	1.54	7.00	1.42
340	0.55	43.62	1.70	54.97	5.88	1.40	4.84	1.16

* Electronic mail: o.j.rolinski@strath.ac.uk

Table 2: Lifetime data extracted from 43 hours of ageing fibrillogenesis model including lifetime values (T1, T2, T3), pre-exponential values (A1, A2, A3), scatter component (Sc), χ^2, and absorbance values for each corresponding wavelength.

Wavelength / nm	T1 / ns	A1 / %	T2 / ns	A2 / %	T3 / ns	A3 / %	Sc / %	χ^2
290	0.45	43.64	1.57	52.62	3.17	3.74	0.00	1.22
295	0.42	39.16	1.48	54.25	2.90	6.59	0.00	1.24
300	0.53	37.83	1.60	58.34	3.44	3.83	5.93	1.16
305	0.49	38.28	1.60	58.93	3.90	2.79	5.17	1.08
310	0.54	37.84	1.61	59.21	3.91	2.95	5.34	1.18
315	0.54	36.89	1.63	60.59	4.16	2.52	5.48	1.08
320	0.44	43.54	1.64	54.83	4.71	1.63	0.00	1.10
325	0.65	41.89	1.74	56.69	5.23	1.42	6.28	1.09
330	0.55	41.67	1.72	56.81	5.24	1.53	3.49	1.16
335	0.59	42.23	1.72	56.35	5.62	1.42	4.79	1.16
340	0.59	42.14	1.73	56.58	6.32	1.28	5.61	1.19

Table 3: Lifetime data extracted from 312 hours of ageing fibrillogenesis model including lifetime values (T1, T2, T3), pre-exponential values (A1, A2, A3), scatter component (Sc), χ^2, and absorbance values for each corresponding wavelength.

Wavelength / nm	T1 / ns	A1 / %	T2 / ns	A2 / %	T3 / ns	A3 / %	Sc / %	χ^2
290	0.44	37.59	1.48	55.24	2.82	7.17	5.90	1.22
295	0.55	38.96	1.62	58.05	3.52	3.00	6.73	1.19
300	0.46	41.88	1.58	54.94	3.52	3.18	0	1.03
305	0.56	40.57	1.67	57.51	4.29	1.92	7.10	1.12
310	0.55	37.67	1.63	59.99	4.19	2.34	6.62	1.18
315	0.49	39.75	1.59	57.34	3.94	2.91	4.45	1.16
320	0.56	43.62	1.67	54.61	4.56	1.77	0.44	1.16
325	0.58	42.19	1.69	56.23	5.01	1.58	5.68	1.10
330	0.58	33.06	1.66	64.64	4.87	2.29	16.21	1.22
335	0.63	44.26	1.74	54.38	5.64	1.36	6.77	1.25
340	0.58	43.03	1.71	55.53	5.96	1.44	6.06	1.18

Table 4: Lifetime data extracted from 454 hours of ageing fibrillogenesis model including lifetime values (T1, T2, T3), pre-exponential values (A1, A2, A3), scatter component (Sc), χ^2, and absorbance values for each corresponding wavelength.

Wavelength / nm	T1 / ns	A1 / %	T2 / ns	A2 / %	T3 / ns	A3 / %	Sc / %	χ^2
290	0.47	40.64	1.54	54.47	3.11	4.89	3.57	1.21
295	0.56	43.15	1.66	54.87	3.95	1.99	2.97	1.12
300	0.46	42.76	1.57	54.09	3.60	3.15	0.00	1.16
305	0.53	39.45	1.63	58.25	4.17	2.29	4.88	1.09
310	0.48	40.07	1.59	57.24	4.03	2.69	2.52	1.11
315	0.52	41.06	1.63	56.72	4.30	2.22	2.51	1.13
320	0.49	41.44	1.62	56.40	4.41	2.17	2.68	1.07
325	0.54	44.31	1.68	53.94	4.80	1.75	2.52	1.13
330	0.60	44.60	1.72	53.97	5.46	1.44	4.48	1.14
335	0.58	46.76	1.72	51.81	5.65	1.42	2.50	1.10
340	0.62	43.69	1.72	54.80	6.12	1.51	5.43	1.14

Table 5: Lifetime data extracted from 693 hours of ageing peptide model including lifetime values (T1, T2, T3), pre-exponential values (A1, A2, A3), scatter component (Sc), χ^2, and absorbance values for each corresponding wavelength.

Wavelength / nm	T1 / ns	A1 / %	T2 / ns	A2 / %	T3 / ns	A3 / %	Sc / %	χ^2
290	1.46	82.83	2.77	32.08	3.08	-14.91	70.28	1.26
295	1.57	93.63	3.97	107.85	4.01	-101.48	41.94	1.14
300	1.55	94.35	3.54	5.66	350	-0.01	22.22	1.22
305	1.55	94.35	3.65	5.66	350	-0.01	13.82	1.14
310	0.67	14.41	1.64	81.21	3.73	4.37	9.13	1.04
315	0.62	14.52	1.63	81.58	3.93	3.90	7.19	1.11
320	1.12	42.67	1.90	55.75	4.99	1.59	6.27	1.16
325	0.55	17.96	1.65	79.21	4.49	2.83	5.03	1.12
330	0.55	21.27	1.69	76.58	5.07	2.15	4.74	1.12
335	0.52	23.88	1.70	74.08	5.42	2.05	4.03	1.14
340	0.75	28.20	1.77	69.98	6.23	1.82	5.44	1.15